Bioorganic & Medicinal Chemistry xxx (xxxx) xxx–xxx

Contents lists available at ScienceDirect

Bioorganic & Medicinal Chemistry

journal homepage: www.elsevier.com/locate/bmc

Tuning the selectivity of *N*-alkylated styrylquinolinium dyes for sensing of G-quadruplex DNA

Ming-Qi Wang[a,*], Jing Xu[a], Lan Zhang[a], Yue Liao[a], Heng Wei[a], Ying-Ying Yin[a], Qiang Liu[b,*], Yuan Zhang[a]

[a] School of Pharmacy, Jiangsu University, Zhenjiang 212013, PR China
[b] College of Chemistry and Environmental Protection Engineering, Southwest Minzu University, Chengdu 610041, PR China

ARTICLE INFO

Keywords:
N-Alkylated styrylquinolinium dye
G-quadruplex DNA
Cytotoxicity
Living HepG2 cell

ABSTRACT

Selective and sensitive detection of G-quadruplex DNA structures is an important issue and attracts extensive interest. To this end, numerous small molecular fluorescent probes have been designed. Here, we present a series of *N*-alkylated styrylquinolinium dyes named **Ls-1**, **Ls-2** and **Ls-3** with varying side groups at the chain end. We found that these dyes exhibited different binding behaviors to DNAs, and **Ls-2** with a sulfonato group at the chain end displayed sensitivity and selectivity to G-quadruplex DNA structures in vitro. The characteristics of this dye and its interaction with G-quadruplex DNA were comprehensively investigated by means of UV–vis spectrophotometry, fluorescence, circular dichroism and molecular docking. Furthermore, confocal fluorescence images and MTT assays indicated dye **Ls-2** could pass through membrane and enter the living HepG2 cells with low cytotoxicity.

1. Introduction

The G-rich single strand DNAs can form polymorphic G-quadruplex structures containing G-quartets stabilized by Hoogsteen hydrogen bonding.[1,2] The whole-genome sequencing experiments and bioinformatics research predict the G-quadruplex forming sequences in the region of human genome such as telomeres, as well as in promoter regions of oncogenes.[3,4] It is believed that the G-quadruplex DNAs play important roles as regulatory elements in many biological processes, especially in regulating gene transcription and translation, and then affected cell proliferation and cancer progression.[5–7] However, up to date, the structures and functions of most G-quadruplex DNAs in genomes are difficult to predict purely. In this context, detection of G-quadruplex DNA structures both in vitro and in vivo is crucial for understanding of their persistence and biological roles.

Fluorescence techniques provide the additional advantage of real-time monitoring of structure and biological functions of biomacromolecules in living cells, with high temporal and spatial resolution.[8] There has been a substantial amount of effort in developing the small molecular fluorescence "light-up" probes to assess the formation and topology of G-quadruplex DNA structures.[9–12] In most cases, these probes like arylvinyl dyes are mostly nonfluorescent in solution alone, due to the rapid nonradiative decay which will be suppressed and give large fluorescence enhancement when binding with G-quadruplex DNAs, for example, through restriction of intramolecular rotation. Since the intramolecular movements of the probes may also be restricted by other nonG-quadruplex DNA forms (e.g. duplex), which will lead to a very poor selectivity. Thus, probes that are capable of detection of G-quadruplex DNAs with a sufficient selectivity over other DNA forms are high desired.

N-Alkylated quinolinium dyes are the common fluorescence molecules used in fluorescence sensing and cell imaging because of their attractive optical properties as well as high DNA binding affinities.[13–20] Moreover, the quinolinium moiety usually plays the role of donor in various systems and can form a D-π-A^+ structure to give a large Stokes shift. The restriction of molecular rotation around the π-conjugated methine bridge between D and A^+ impacts the push–pull effects, and this process can be specific to a conformation of G-quadruplex, giving rise to different spectroscopy responses. Our group reported a series of quinolinium-based D-π-A^+ fluorescent probes and studied their effects for selective G-quadruplex DNA targeting.[21–23] Structure-activity studies indicated that the positively charged quinolinium scaffold would interact with the DNA base by π-π stacking or with the phosphate backbone *via* electrostatic interactions. In particular, systematically changing the side chains of the quinolinium scaffold is a facile pathway to increase the binding affinity and selectivity to G-quadruplex DNA, as

* Corresponding authors.
E-mail addresses: wmq3415@163.com (M.-Q. Wang), lqchem@163.com (Q. Liu).

https://doi.org/10.1016/j.bmc.2018.12.037
Received 8 October 2018; Received in revised form 14 December 2018; Accepted 27 December 2018

well as to modulate the cellular uptake. However, the effect on the substitutions on the quinoline nitrogen atom for detection of G-quadruplex is rarely found in literature. Upon further investigation of this series, in the present study, we designed three *N*-alkylated styrylquinolinium dyes **Ls-1**, **Ls-2** and **Ls-3** with different groups at the chain end. Their photophysical characterization and fluorescence performance on various DNA forms were investigated. These dyes were able to bind with nucleic acids, and dye **Ls-2** with a sulfonato group at the chain end displayed excellent fluorescent signal discrimination to G-quadruplex DNA. The detailed binding properties for G-quadruplex DNA were assessed through both experimental and modeling studies. In addition, the intracellular localization and cytotoxicity were also explored.

2. Experimental methods

2.1. Materials and methods

4-Methyl-1-(4-sulfobutyl)quinolinium inner salt,[24] 1-(3-hydroxypropyl)-4-methyl-quinolinium iodide[25] and 1,4-dimethyl-quinolinium iodide[13] were synthesized according to previously described literature protocols. All commercially available chemicals, solvents, used for synthesis, were reagent grade and used without further purification. All oligonucleotides were purchased from Sangon Biotechnology Co., Ltd. (Shanghai, China) and their sequences were listed in Table S1. All the oligonucleotides were dissolved in Tris − HCl buffer (10 mM, containing 60 mM KCl, pH 7.4). Stock solutions of **Ls-1**, **Ls-2** and **Ls-3** were prepared in DMSO. ^{1}H NMR and ^{13}C NMR spectra were measured on a 400 MHz spectrometer (400 MHz for ^{1}H and 100 MHz for ^{13}C) using TMS as internal standard in DMSO-d_6. High resolution mass spectra (HRMS) were recorded on a Shimazu LCMS-IT-TOF instrument with an ESI detector.

2.2. General method for preparation of quinolinium derivatives

4-(4-Methylpiperazino)benzaldehyde (1.1 mmol) and quinolinium salts (1.0 mmol) were added to a 100 mL flask with 40 mL anhydrous ethanol, followed by 5 drops catalytic piperidine. The resulting mixture was allowed to reflux for 15 h under nitrogen with stirring. After cooling to room temperature, the solvent was removed under reduced pressure and the residue was purified by column chromatography on silica gel eluting with CH_2Cl_2/CH_3OH to afford quinolinium derivatives as a brownish solid.

2.2.1. Characterization of *Ls-1*

Yield 43.5%, ^{1}H NMR (400 MHz, DMSO-d_6) δ: 9.34 (d, J = 6.56 Hz, 1H), 9.06 (d, J = 8.60 Hz, 1H), 8.48 (d, J = 8.96 Hz, 1H), 8.40 (d, J = 6.68 Hz, 1H), 8.20–8.16 (m, 2H), 8.08–8.04 (m, 1H), 7.96 (t, J = 8.08 Hz, 1H), 7.88 (d, J = 8.72 Hz, 2H), 7.03 (d, J = 8.80 Hz, 2H), 5.13 (s, 1H), 5.02 (t, J = 6.92 Hz, 2H), 3.52–3.37 (br, 10H), 2.26 (s, 3H), 2.10–2.07 (m, 2H); ^{13}C NMR (100 MHz, DMSO-d_6) δ: 153.68, 152.92, 147.41, 144.63, 138.31, 135.25, 131.52, 129.05, 127.28, 126.76, 125.74, 119.40, 115.29, 115.19, 114.66, 60.21, 57.83, 54.50, 54.27, 21.24, 14.56; HRMS: (positive mode, m/z) calculated 388.2383, found 388.2349 for [M-I]$^{+}$;

2.2.2. Characterization of *Ls-2*

Yield 51.1%, ^{1}H NMR (400 MHz, DMSO-d_6) δ: 9.24 (d, J = 6.72 Hz, 1H), 9.04 (d, J = 8.08 Hz, 1H), 8.54 (d, J = 8.92 Hz, 1H), 8.39 (d, J = 6.72 Hz, 1H), 8.20–8.14 (m, 2H), 8.09–8.05 (m, 1H), 7.98 (t, J = 7.76 Hz, 1H), 7.88 (d, J = 8.96 Hz, 2H), 7.06 (d, J = 8.96 Hz, 2H), 4.94 (t, J = 7.24 Hz, 2H), 3.38–3.33 (m, 4H), 2.49–2.44 (m, 6H), 2.23 (s, 3H), 2.05–1.99 (m, 2H), 1.73–1.65 (m, 2H); ^{13}C NMR (100 MHz, DMSO-d_6) δ: 153.69, 153.01, 147.02, 144.65, 138.33, 135.31, 131.50, 129.12, 127.14, 126.76, 125.68, 119.58, 115.25, 114.65, 56.45, 54.66, 52.71, 51.04, 50.89, 46.94, 45.96, 28.91, 23.31, 22.98, 22.64; HRMS: (positive mode, m/z) calculated 466.2164, found 466.2162 for [M + H]$^{+}$.

2.2.3. Characterization of *Ls-3*

Yield 67.3%, ^{1}H NMR (400 MHz, DMSO-d_6) δ: 9.19 (d, J = 6.68 Hz, 1H), 9.06 (d, J = 8.16 Hz, 1H), 8.39–8.36 (m, 2H), 8.25–21 (m, 1H), 8.18–8.14 (m, 1H), 8.11–8.07 (m, 1H), 8.02 (t, J = 7.52 Hz, 1H), 7.89 (d, J = 8.96 Hz, 2H), 7.07 (d, J = 8.96 Hz, 2H), 4.47 (s, 3H), 3.38–3.36 (m, 4H), 2.49–2.47 (m, 4H), 2.24 (s, 3H); ^{13}C NMR (100 MHz, DMSO-d_6) δ: 153.48, 152.42, 147.71, 144.19, 139.23, 135.23, 131.40, 129.28, 126.93, 126.42, 126.17, 119.64, 115.62, 115.25, 115.00, 53.81, 46.09, 44.82, 44.59, 44.24, 22.67, 22.05; HRMS: (positive mode, m/z) calculated 344.2121, found 344.2083 for [M-I]$^{+}$;

2.3. Measurements and methodology

2.3.1. Spectrophotometric studies

The absorption spectra were recorded on an UV-2550 spectrophotometer using a 1 cm path length quartz cuvette at room temperature. For the titration experiment, small aliquot of a stock solution of DNA was added to the solution containing the dye at a fixed concentration (8 μM) in aqueous buffer (10 mM Tris-HCl, pH 7.4, 60 mM KCl). After each DNA addition, the solution was incubated for 2 min before absorption spectra recorded.

2.3.2. Fluorimetric titrations

Fluorescence spectra were measured on a Shimadzu RF-5301PCS spectrofluorophotometer in a 10 mm quartz cell at room temperature. The concentration of the dye was fixed at 2 μM and the titration process was similar to absorption spectra titration experiment. The date from the fluorimetric titrations were analyzed according to the independent-site model by nonlinear fitting to Eq. (1),[26] in which F_0 is the fluorescence intensity of the dye in the absence of G-quadruplex DNA, n is the putative number of the dye binding to a given DNA matrix, Q is the fluorescence enhancement upon saturation, $A = 1/[K_a C_{dye}]$ and $x = nC_{DNA}/C_{dye}$. The parameters Q and A were found by Levenberg-Marquardt fitting routine in Origin 8.5 software.

$$\frac{F}{F_0} = 1 + \frac{Q-1}{2}[A + 1 + x - \sqrt{(A+1+x)^2 - 4x}] \quad (1)$$

2.3.3. Circular dichroism (CD)

CD spectra (230–500 nm) were performed on a JASCO-J815 circular dichroism spectrophotometer using a 10 mm path length quartz cuvette at 25 °C. The scanning speed of the instrument was set to 500 nm min^{-1}. The strand concentration of G-quadruplex used for measurement was 4 μM. CD signals were recorded with a band width of 1 nm and final analysis of the data was carried out using Origin 8.5.

2.3.4. Molecular docking

Molecular docking calculations were performed using the Autodock Vina software, which has been reported to be of high accuracy of prediction.[27] The crystal structure (PDB code: 1KF1, resolution: 2.10 Å) and the NMR structure (PDB code: 143D) of G-quadruplex DNA were downloaded from RCSB Protein Data Bank. The redundant solvent molecules and ions were removed from the crystal structure while the first conformation was retained from the NMR structure. Docked poses were visualised by using UCSF Chimera.

2.3.5. Fluorescence intercalator displacement (FID) assays

FID assays were also performed on a Shimadzu RF-5301PCS spectrofluorophotometer. The experiments were carried out in 10 mM Tris-HCl buffer (pH 7.4, containing 60 mM KCl) by adding different concentrations of dyes to the TO-bound G-quadruplex solution. The concentrations of TO and G-quadruplex were set at 0.5 and 0.25 μM, respectively. The fluorescence spectra were measured using excitation

wavelength at 504 nm and the emission range was set between 520 and 700 nm.

2.3.6. Activity inhibition experiment of G4/Hemin peroxidase

The peroxidase inhibition experiments were recorded on an UV-2550 spectrophotometer using a 1 cm path length quartz cuvette at room temperature. 10 μL of 100 μM G-quadruplex sequence mixed with/without **Ls-2** (2–10 μL of 2.5 mM) to a volume of 2.5 mL Tris-HCl buffer solution. After standing for 1 h at room temperature, the resulting solutions were mixed with 1 μL of 2.5 mM hemin and incubated for another 1 h. Then 15 μL of 30 mM ABTS was added, reactions were initiated by addition of H_2O_2 (15 μL of 30 mM). The absorbance was determined at 415 nm immediately within 30 min.

2.3.7. Cytotoxicity assay

The human hepatocellular liver carcinoma cells (HepG2) were cultured in DMEM containing high glucose (5.5 mM) supplemented with 10% FBS at pH 7.4. Cells were maintained in tissue culture plates at 37 °C in an atmosphere of 5% CO_2. The cancer cells were treated with various concentrations (1, 10, 100, and 150 μM) of dye **Ls-2** for 24 h and 48 h. Cell viability was determined by MTT assay. 20 μL of MTT (5 mg/mL in PBS buffer) was added to each well and further incubated for 4 h. The cells in each well were then treated with DMSO (150 μL for each well) and the optical density (OD) was recorded at 570 nm.

2.3.8. Living and fixed cells staining experiment

Confocal fluorescence imaging was obtained in living and fixed HepG2 cells, which was recorded on a LSM 710 laser scanning confocal microscope. For living cells imaging, cells were grown on confocal dishes for 24 h, after washing with PBS, the cells were incubated with **Ls-2** (20 μM) for 0.5 h at 37 °C. The stained cells were washed with PBS and observed under the confocal microscope. For fixed cells imaging, cells were fixed with 4% paraformaldehyde in PBS for 15 min, then were subsequently incubated with 20 μM of **Ls-2** for 0.5 h at 37 °C. The living and fixed cells were also stained with DAPI (5 μg/mL) for 30 min at 37 °C. The excitation wavelengths were 405 nm for DAPI and 480 nm for **Ls-2**, respectively.

3. Results and discussion

3.1. Synthesis of new fluorescence dyes

As shown in Scheme S1, the dyes **Ls-1**, **Ls-2** and **Ls-3** were synthesized through condensation of 1-(3-hydroxypropyl)-4-methyl-quinolinium iodide, 4-Methyl-1-(4-sulfobutyl)quinolinium inner salt and 1,4-dimethyl-quinolinium iodide, respectively, with 4-(4-Methylpiperazino)benzaldehyde according to the established protocols.[21–23] The structures of these new dyes were characterized by ^{1}H NMR, ^{13}C NMR and HRMS (see the Supplementary Information).

3.2. Photophysical properties

With the dyes in hand, the solvatochromic properties in different solvents of varying polarity were first investigated by using an UV–Vis spectrophotometer and a fluorescence spectrophotometer. The electronic absorption and fluorescence emission spectra were obtained at concentration of 10 μM (Fig. 1). All the three dyes showed the shortest absorption wavelength in buffer solution and the longest in DMSO. In protic solvents the spectra of the three dyes exhibited a blue shift of the λ_{max} with the increase of solvent polarity, while in the aprotic solvents the dyes underwent a relatively modest red shift. The effect of the protic solvent polarity on λ_{max} can be illustrated by the interactions between the dye and the solvents, as the interaction makes the ground state of the dye more stable than the excited state by forming hydrogen bonds.[28,29] Increasing the aprotic solvent polarity stabilizes the excited state relative to the ground state with the observed red shift of λ_{max}.[30] From the emission spectra, we can see that each dye exhibited a solvent-dependent emission behavior. Emission intensity of **Ls-2** was dramatically decreased with the increasing solvent polarity and was the lowest in buffer solution, and the behaviors of dyes **Ls-1** and **Ls-3** are similar to that of dye **Ls-2**. The possible reason is that the rotational mobility of the aromatic moieties around the C=C bond changed in conjunction with polarity effects. In addition, all the dyes have large Stokes shifts in various solutions, especially in buffer solution. The maximum value reached to 200 nm in buffer. Thus, these dyes may play a key role in avoiding self-quenching in process of biological applications.

3.3. Screening of the N-alkylated styrylquinolinium dyes: *Ls-1, Ls-2 and Ls-3*

The fluorimetric response of *N*-alkylated styrylquinolinium dyes: **Ls-1**, **Ls-2** and **Ls-3** on different kinds of nucleic acids was initially investigated. 11 representative oligonucleotides, including G-quadruplex DNA, single-stranded and double-stranded DNA were employed in the assays. The experiments were performed in K^+-rich conditions (60 mM), using a concentration of 2 μM of dyes, and DNA-to-dye ratio of 5:1. The excitation wavelength for the three dyes was fixed at isosbestic point (480 nm) which identified by UV–Vis titration experiments (Figs. S1–3). As shown in Fig. 2, with addition of DNA, the fluorescence intensity of the three dyes increased, suggesting there were certain interactions between DNA and dyes. According to the enhanced times of fluorescence signals, the two dyes **Ls-1** and **Ls-3** showed significant fluorescence enhancements in the presence of certain G-quadruplex DNA targets, in particular of the parallel topology group (CM22, C-myc). However, similar fluorescence enhancements were also observed in the presence of nonG-quadruplex DNAs, which demonstrated dyes **Ls-1** and **Ls-3** gave poor discrimination of G-quadruplex DNA structures. In contrast, the fluorescence intensity of **Ls-2** with a negatively charged sulfonato group presented an obvious enhancement upon binding to G-quadruplex DNA, whereas exhibited much lower fluorescence signal after interacting with nonG-quadruplex DNA, demonstrated its capacity to serve as G-quadruplex DNA probe. Evidently, alternation in the structure of *N*-alkyl chains dramatically affects the emission of the dye, indicative of geometric structure matching in the binding process of the dyes with the quadruplex DNA. Thus, **Ls-2** was chosen for further detailed investigation.

3.4. Fluorescence properties of *Ls-2* with DNA forms

Since G-quadruplex DNA caused a strong enhancement of fluorescence spectra in **Ls-2**, the detailed fluorescence properties of **Ls-2** with various DNAs were explored *via* a fluorimetric titration assay. As shown in Fig. 3**A**, **Ls-2** (2 μM) alone in buffer displayed very weak fluorescence intensity. With gradual addition of G-quadruplex DNA CM22 (0–3 μM), the emission peak at approximately 630 nm was significantly enhanced, which caused about 145-fold fluorescence enhancement. This fluorescent light-up property was also observed when treated with other G-quadruplex DNA (22AG 100-fold, HTG-21 120-fold, C-myc 118-fold, G3T3 103-fold, HRAS 134-fold at saturation) (Fig. S4). In contrast, only weak fluorescence enhancements from 10- to 40-fold were observed when titrating **Ls-2** with single-stranded DNA (ss26), double-stranded DNA (CTDNA, ds26, Polyd(A-T)$_9$ and Polyd(G-C)$_9$). In order to examine whether the significant fluorescence enhancement of **Ls-2** was due to its interactions with G-quadruplex secondary structure or just simply G-rich sequence, we used mutated CM22 single-stranded sequences as control groups. Mutation of guanines in this sequence abrogates the formation of the G-quadruplex structure. Following a similar titration protocol (Fig. 3B), the fluorescence enhancements of the mutated sequences were found to be much lower than that of CM22 G-quadruplex, which demonstrated that **Ls-2** indeed interacted with G-quadruplex secondary structure instead of simple G-rich sequence. In addition, it is

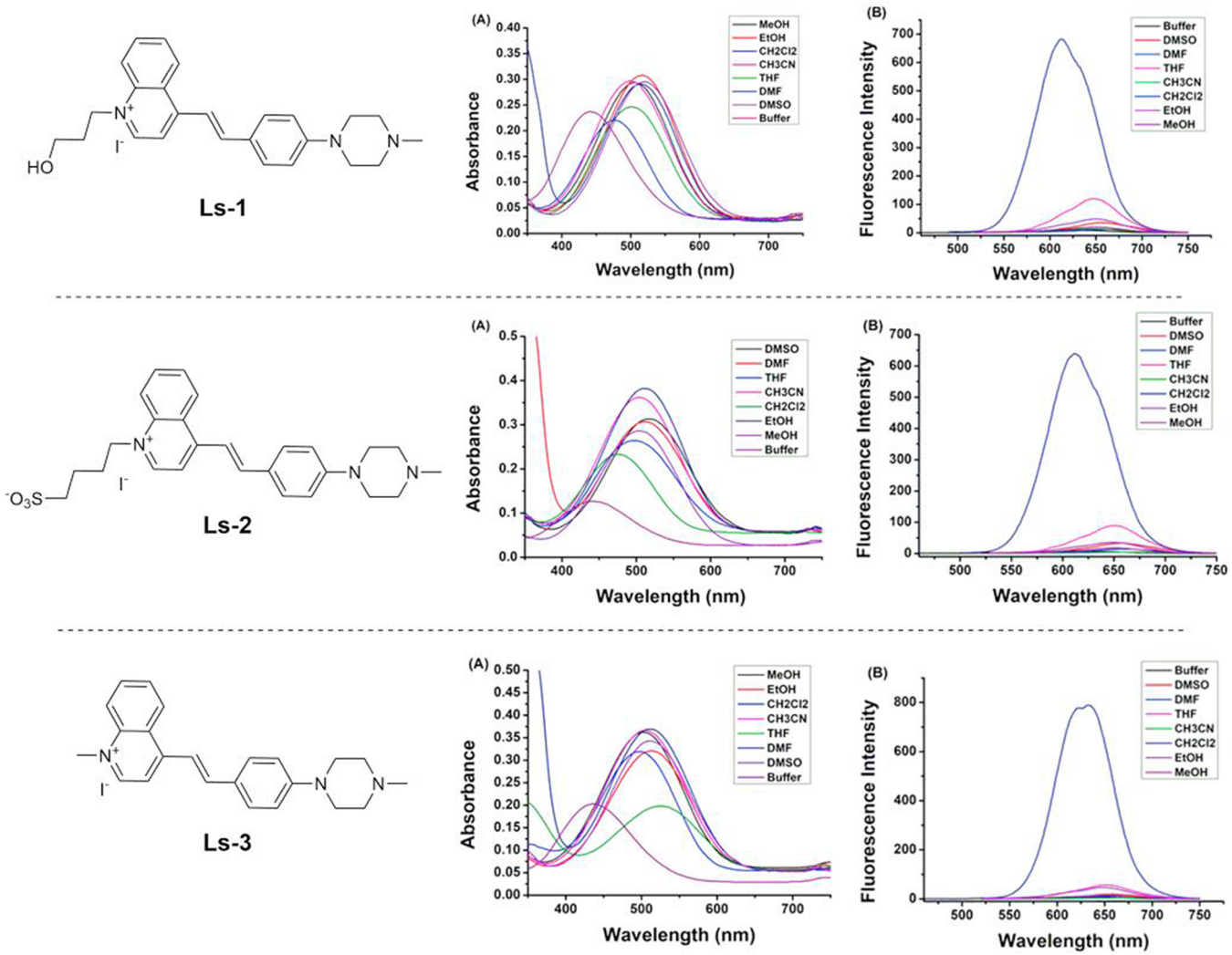

Fig. 1. Absorption and fluorescence spectra of **Ls-1**, **Ls-2** and **Ls-3** in various solvents. [**Ls-1**] = [**Ls-2**] = [**Ls-3**] = 10 μM. **Ls-1**/**Ls-2**/**Ls-3**: λ_{ex} (DCM) = 477/477/498 nm; λ_{ex} (THF) = 501/499/507 nm; λ_{ex} (CH_3CN) = 500/504/505 nm; λ_{ex} (Buffer) = 441/441/436 nm; λ_{ex} (MeOH) = 506/506/503 nm; λ_{ex} (EtOH) = 517/510/510 nm; λ_{ex} (DMSO) = 520/517/511 nm; λ_{ex} (DMF) = 514/511/511 nm.

worth pointing out that the far-red (600–750 nm) region emission of **Ls-2** with G-quadruplex DNA is sought-after due to minimal auto-fluorescence and cellular damage. Taken together, **Ls-2** displayed promising application prospects for the special detection of G-quadruplex DNA structures.

*3.5. Absorption spectral titration studies of **Ls-2** interactions with DNA forms*

The ability of **Ls-2** to interact both G-quadruplex and other DNAs was also studied by spectrophotometric titration experiments. In dilute

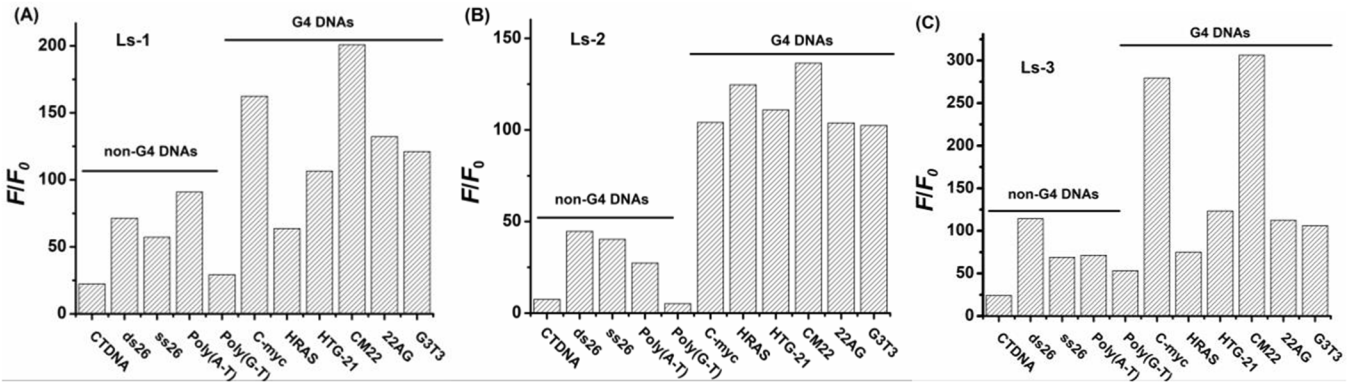

Fig. 2. Fluorescence responses of 2 μM of **Ls-1**, **Ls-2**, and **Ls-3** to 10 μM of different DNAs ($\lambda_{ex}/\lambda_{em}$ = 480/630 nm) in 10 mM of Tris-HCl buffer and 60 mM of KCl at a pH of 7.4.

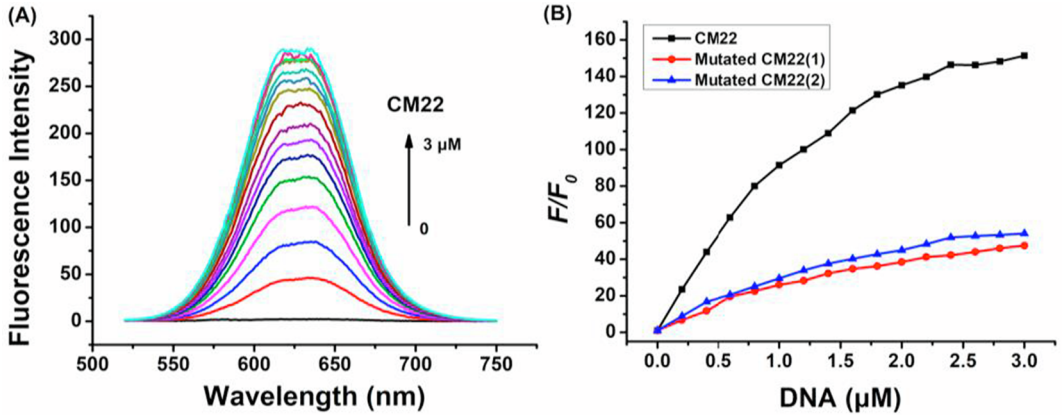

Fig. 3. (A) Fluorescence titration of 2 μM of **Ls-2** with stepwise addition of the G-quadruplex-forming oligonucleotide (CM22, arrows: 0–3 μM) in 10 mM of Tris-HCl buffer and 60 mM of KCl at a pH of 7.4. (B) Fluorescence intensity enhancement of **Ls-2** (2 μM) versus concentrations of G-quadruplex DNA CM22 and mutated CM22 single-stranded sequences.

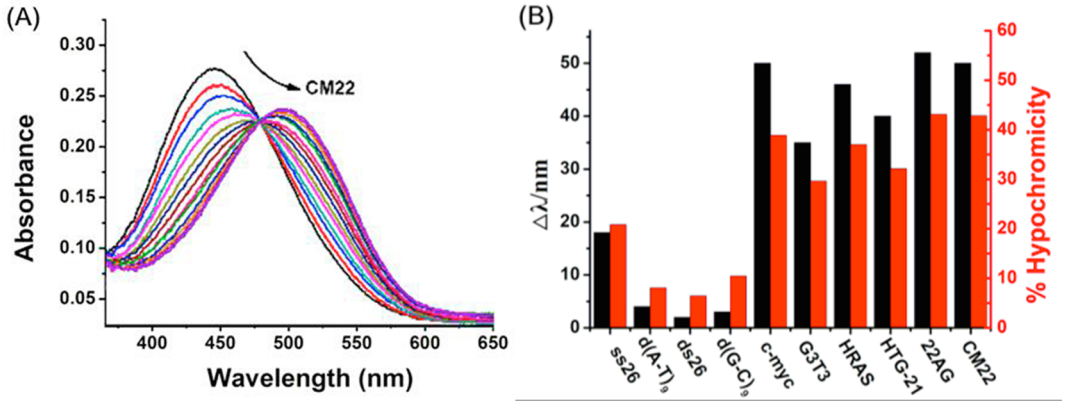

Fig. 4. (A) Absorption spectra of **Ls-2** (8 μM) upon addition of CM22. [CM22] = 0–3 μM from top to bottom. Arrows indicate the change in absorbance upon increasing the CM22 concentrations. (B) Absorbance response of **Ls-2** to DNAs, the black bar corresponds to the shift in the absorbance maximum (λ_{max}) and the red bar corresponds to the hypochromicity (%).

solution of **Ls-2**, it displayed its characteristic absorption profile with a maximum at 443 nm (Fig. 4A). In the presence of DNA, the red shift (△λ) and hypochromic effect (%H) of maximum absorbance are observed (Figs. S2 and S8) and their values are summarized in Fig. 4B. Notably large hypochromicities (30.1–43.2%) and red shifts (35–52 nm) with clear isosbestic points are observed for **Ls-2** with addition of G-quadruplex DNAs, and these spectral features indicated there was π-π stacking between the dye aromatic core and the external G-quartets in the binding process. On the other hand, the effect of single- and double-stranded DNAs on the absorption bands of **Ls-2** was much smaller than G-quadruple DNAs. Of note, the redshift of the absorption band of the dye was larger in the case of G-quadruplex structure, pointing out the differences in the dye-binding sites (geometry, polarity) in non-G-quadruplex DNA and G-quadruplex DNA. Also, hypochromism indicates the binding affinity between the chromophore and DNA bases. The stronger hypochromicity suggested that **Ls-2** had much stronger interaction with G-quadruplexes than with other DNA forms, which was consistent with the results of fluorescence spectra. The presence of a clean-cut isosbestic point suggests a 1:1 complexation between **Ls-2** and G-quadruplex DNA, and this was further confirmed by Job's plot analysis (Fig. S5). Taken together, the combination of two outputs (fluorescence and absorption) proves **Ls-2** could also be used as a selective probe to distinguish G-quadruplexes from other DNA forms.

3.6. Binding properties

Besides selectivity, sensitivity is another crucial parameter to assess the performance of the designed probes. Therefore, we also investigated the detection limits (LODs) of **Ls-2** for different G-quadruplexes according to the equation $3\sigma/k$.[26] Good linearity between the fluorescence intensity and the most of G-quadruplex DNAs in the range of 0.1–1.0 μM were obtained. The corresponding LOD values of **Ls-2** for G-

Table 1
Apparent binding constants (K_a), binding stoichiometry (n) and the detection limits (LOD) of **Ls-2** to different G-quadruplex DNAs, determined from fluorimetric titrations.

G-quadruplex DNA[a]	Stoichiometry (**Ls-2**:DNA)	K_a [10^6 M^{-1}]	Lrd (μM)[b]	LOD (nM)
22AG	1:1	0.41	0–0.8	17.4
CM22	1:1	1.81	0–0.8	8.8
C-myc	1:1	2.22	0–1.0	11.2
Htg-21	1:1	0.45	0–1.0	16.6
HRAS	1:1	0.83	0–1.4	37.7
G3T3	1:1	1.15	0–0.8	9.1

[a] Experimental conditions: **Ls-2** = [2 μM] in 10 mM Tris-HCl buffer (pH 7.4) containing 60 mM KCl.
[b] Linear detection range.

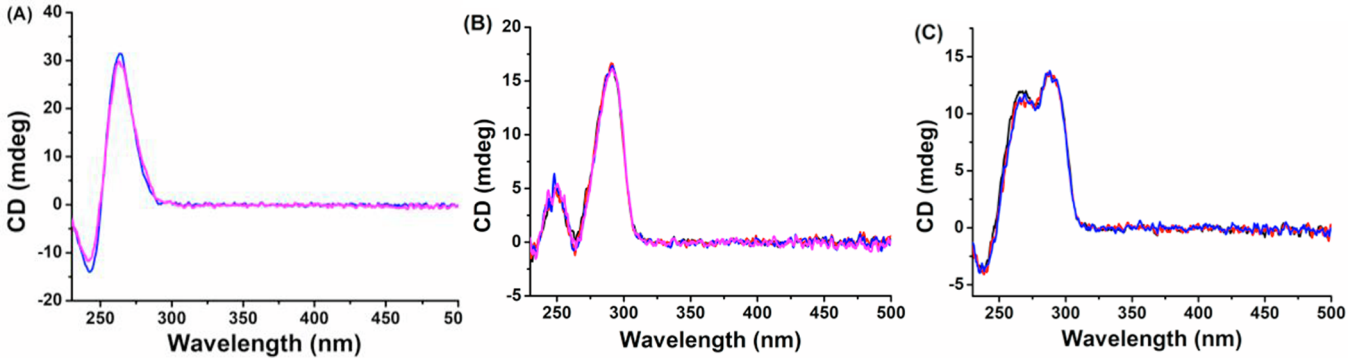

Fig. 5. CD spectra of 5 μM G-quadruplex-forming oligonucleotides CM22 (A), HRAS (B), and Htg-21 (C) in 10 mM Tris-HCl buffer, 60 mM KCl, pH 7.4 with and without **Ls-2** (0–10 μM).

quadruplex 22AG, CM22, C-myc, G3T3, HRAS and HTG-21 were 17.4 nM, 8.8 nM, 11.2 nM, 9.1 nM, 37.7 nM, and 16.6 nM, respectively (Table 1 and Fig. S6). Clearly, the LODs of **Ls-2** for different G-quadruplex DNAs in solution were in the nanomolar range.

In order to gain insights into the detail binding affinity, we evaluated the binding constants (K_a) and stoichiometries (n) between **Ls-2** and G-quadruplexes using fluorescence titration curves which were further fitted to an independent-site model (Fig. S7). The results (Table 1) indicated that, among the six G-quadruplex DNAs, **Ls-2** displayed higher binding affinity for parallel topology group (C-myc, CM22) than other groups. The results were in agreement with the correlation between fluorescence titration data and LOD values, suggesting that **Ls-2** may show some preference among different G-quadruplex DNA topologies.

3.7. CD spectroscopy

Binding of dyes to G-quadruplex DNA structures may induce conformation changes of the latter, and circular dichroism (CD) spectroscopy is a perfect technique for tracing the conformational transitions of G-quadruplex structures. To assess the interaction between dyes and G-quadruplex, we compared CD spectra of several belonging to different topological groups (parallel, anti-parallel and hybrid) in the absence/presence of **Ls-2**. At the employed conditions (60 mM K^+), all G-quadruplex DNAs showed CD spectra typical of their topologies (Fig. 5). With addition of **Ls-2** to G-quadruplex solutions, the locations and intensities of characteristic peaks failed to change, indicating **Ls-2** can sense G-quadruplexes without affecting the G-quadruplex topologies.

3.8. Binding mechanism

To investigate the binding mode between **Ls-2** and G-quadruplex structures, fluorescence intercalator displacement (FID) and G4/hemin peroxidase inhibition experiments were first performed. FID assay utilizes a probe thiazole-orange (TO), which is virtually nonfluorescent in the free state and becomes strongly fluorescent upon binding to quadruplex DNA.[31] It is reported that TO mainly bound to G-quadruplex DNA by an end-stacking mode. If the ligand with a same binding site, it will compete with TO from the DNA target resulting in the large decrease of the emission. Fig. S9 shows the fluorescence spectra of gradual addition of **Ls-2** to TO-G-quadrurplex solutions. Only a little displacement of TO was detected, implied the presence of an indirect evidence that the grooves/loops binding mode between **Ls-2** and G-quadruplex DNA. Similarly, hemin is also regarded to bind with G-quadruplex structure by end-stacking and consequently possesses catalytic activity on the oxidation of $ABTS^{2-}$ by H_2O_2, which will lead to increase the absorbance at 415 nm.[32] As expected (Fig. 6), compared with control, in the excess of **Ls-2**, the peroxidase activity was a little inhibited, which

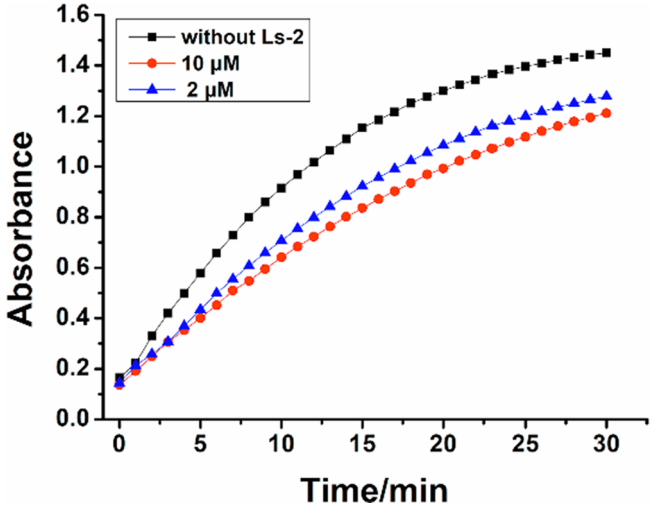

Fig. 6. Inhibition activity of **Ls-2** on the peroxidase activity of G4/hemin complexes.

indicating that **Ls-2** bound with G-quadruplex by grooves/loops mode.

To gain further insight into the interactions of **Ls-2** and G-quadruplexes, molecular docking studies were carried out by using AutoDock Vina modeling tool. The anti-parallel basket NMR G-quadruplex structure (PDB 143D) and a parallel-type crystal G-quadruplex structure (PDB 1KF1) were used as the templates for the docking studies (Fig. 7). The docking results showed that **Ls-2** binds to the anti-parallel quadruplex (143d) in the groove region. The nucleobases DG-2, DG-3, DG-4, DG-8, DG-9 and DG-10 were associated with the highest number of productive contacts. In this mode, the piperazine unit interacts with the groove regions. The quinolinium and benzene moieties exhibited a CH-π stacking interaction with the DG3 nucleobase. The best docking orientation of **Ls-2** with 143d shows an interaction energy value of −5.9 kcal/mol. Another model 1kf1 (parallel structure) with interaction energy of −7.5 kcal/mol also indicates possible interaction of **Ls-2** with the groove regions. The piperazine and benzene moieties bind to the quadruplex groove and loop region formed by nucleobases DG-16, DT-17, DA-19, DG-20 and DG-21. The quinolinium moiety exhibited a π-π stacking interaction with the DG16 nucleobase. In both the models, the sulfonato group was found to participate a hydrogen bonding with the nucleobases. These data indicated that **Ls-2** might bind to the G-quadruplex in a groove binding mode, and exhibited stronger stabilizing ability for the parallel structure than the anti-parallel structure. These were in agreement with observations of the changes in the fluorescence spectra.

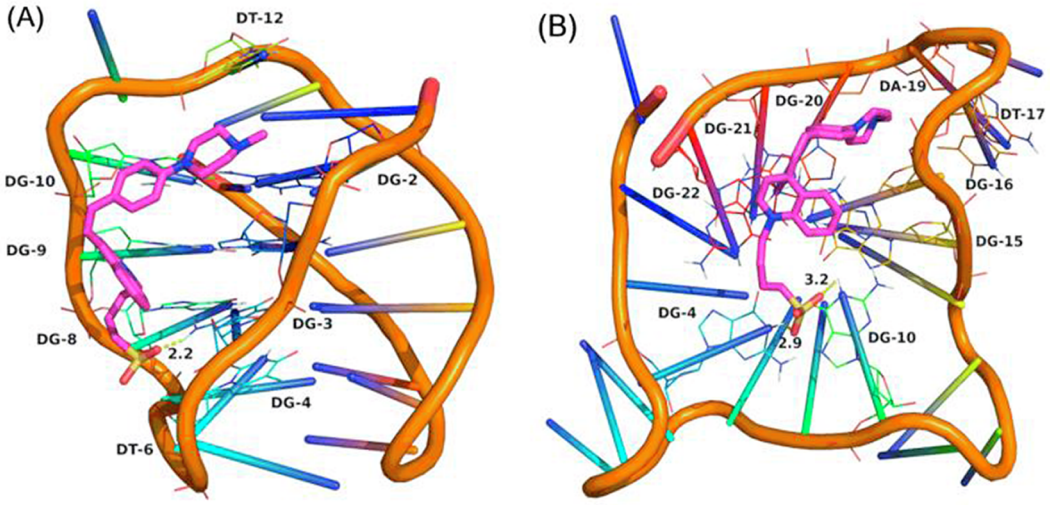

Fig. 7. (A) Molecular modeling for **Ls-2** and anti-parallel G-quadruplex 143 d; (B) Molecular modeling for **Ls-2** and parallel G-quadruplex 1kf1.

Table 2
MTT cell viability assay showing IC50 values of **Ls-2** over 24–48 h in Hep-G2 cells.

IC_{50} Values (μM)		
	24 h	48 h
Ls-2	> 150	> 150

3.9. Application of *Ls-2* in cellular imaging

Low cytotoxicity is one of the most critical requirements for fluorescent probes. The cytotoxicity of probe **Ls-2** was measured using a standard MTT [3-(4, 5-dimethylthiazol)-2, 5-diphenyltetrazolium bromide] method to evaluate the potential application in live cell imaging. Human liver hepatocellular carcinoma cells (HepG2) was incubated with **Ls-2** at a concentration range from 0 to 150 μM for 24 h and 48 h, and the cytotoxic effect is shown in Table 2. It clearly showed that **Ls-2** exhibited almost no toxicity towards HepG2 cell line even at relatively high concentration (150 μM). In fact, cells for bioimaging were exposed to a quite low concentration (0.5 μM) of the probes. The results suggested that **Ls-2** should be safe when used for bioimaging of G-quadruplex DNAs.

Further, fluorescence imaging experiments of dye **Ls-2** in live and fixed HepG2 cells were carried out using confocal fluorescence microscopy to detect the ability of cell permeability and cellular localization. We stained live and fixed HepG2 cells with 20 μM of the tested **Ls-2**, and with 5 mg/mL DAPI (duplex DNA probe) respectively (Fig. 8). Staining of live cells confirmed that **Ls-2** could enter living cells. The co-staining with DAPI in both live and fixed cells showed that **Ls-2** mainly located in cytoplasm. As a selective fluorescent probe for G-quadruplex DNA in vitro, the fluorescence signal of **Ls-2** was not found in nucleus. The fluorescence from the cytoplasm may be due to some reasons: 1) G-quadruplex formation in gene occurs transitorily when

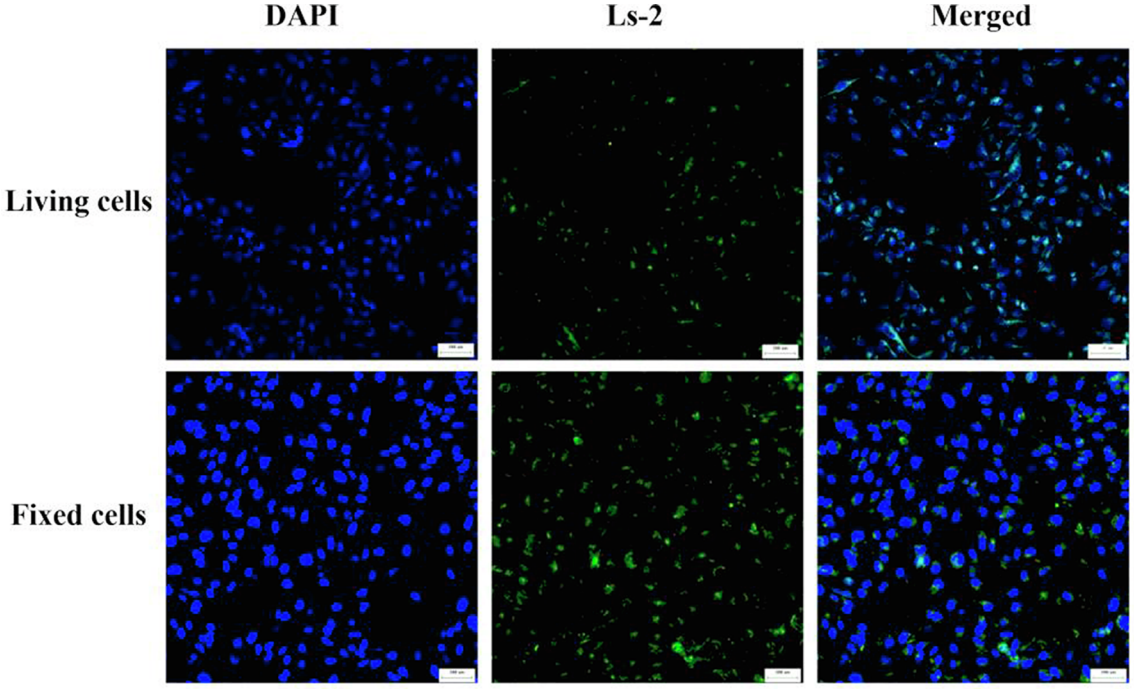

Fig. 8. Confocal fluorescence images of living and fixed Hep-G2 cells stained with 20 μM **Ls-2** and 5 mg/mL **DAPI** for 30 min using a 480 nm laser. Scale bar is 20 μm.

the double-stranded DNA is actively denatured during transcription and replication, the fluorescence of **Ls-2** upon binding to G-quadruplex might be hardly observed. 2) It may be due to the poor nuclear membrane permeability of **Ls-2**. Further we will focus on the structure modification of this scaffold for enhancing its ability of sensing G-quadruplexes in cellular.

4. Conclusion

Rational design of highly selective fluorescent probes to detect G-quadruplexes is of profound importance for basic research. On this basis, we designed and synthesized a series of *N*-alkylated styrylquinolinium dyes **Ls-1**, **Ls-2** and **Ls-3**. Among these dyes, **Ls-2** which carried a sulfonato group at the chain end was chosen as the most promising candidate due to its significant absorbance shift and fluorescence enhancement in the presence of G-quadruplex DNA and insignificant change with non-G-quadruplex structure. The interactions between **Ls-2** and G-quadruplex DNA have been investigated in detail. Our results demonstrated that **Ls-2** interacted with G-quadruplex DNAs mainly by the groove binding mode without affecting their topologies and exhibited higher binding affinity to parallel G-quadruplexes. Furthermore, we also assessed the behavior of **Ls-2** in cellular application. **Ls-2** could enter into living cells and mainly locate in cytoplasma with low cytotoxicity. Taken together, this work provides successful example of developing probes for targeting G-quadruplex DNA *via* the rational structural modification. Further investigations will focus on the work of detection and visualization of G-quadruplex structures in cells.

Acknowledgements

This work was financially supported by the Natural Science Foundation of Jiangsu Province (BK20180857), General Program of Natural Science Foundation of the Higher Education Institutions of Jiangsu Province (17KJB150009) and China Postdoctoral Science Foundation Funded Project (2017M611704).

Appendix A. Supplementary data

Supplementary data to this article can be found online at https://doi.org/10.1016/j.bmc.2018.12.037.

References

1. Burge S, Parkinson GN, Hazel P, Todd AK, Neidle S. Quadruplex DNA: sequence, topology and structure. *Nucl Acids Res.* 2006;34:5402–5415.
2. Bhattacharyya D, Mirihana Arachchilage G, Basu S. Metal cations in G-quadruplex folding and stability. *Front Chem.* 2016;4:38.
3. Huppert JL. Structure, location and interactions of G-quadruplexes. *FEBS J.* 2010;277:3452–3458.
4. Huppert JL, Balasubramanian S. Prevalence of quadruplexes in the human genome. *Nucl Acids Res.* 2005;33:2908–2916.
5. Tian T, Chen YQ, Wang SR, Zhou X. G-quadruplex: a regulator of gene expression and its chemical targeting. *Chemistry.* 2018;4:1314–1344.
6. Rhodes D, Lipps HJ. G-quadruplexes and their regulatory roles in biology. *Nucl Acids Res.* 2015;43:8627–8637.
7. Cao Q, Li Y, Freisinger E, Qin PZ, Sigel RKO, Mao ZW. G-quadruplex DNA targeted metal complexes acting as potential anticancer drugs. *Inorg Chem Front.* 2017;4:10–32.
8. Suganya S, Naha S, Velmathi S. A critical review on colorimetric and fluorescent probes for the sensing of analytes via relay recognition from the year 2012–17. *Chemistryselect.* 2018;3:7231–7268.
9. Duarte AR, Cadoni E, Ressurreicao AS, Moreira R, Paulo A. Design of modular G-quadruplex ligands. *ChemMedChem.* 2018;13:869–893.
10. Suseela YV, Narayanaswamy N, Pratihar S, Govindaraju T. Far-red fluorescent probes for canonical and non-canonical nucleic acid structures: current progress and future implications. *Chem Soc Rev.* 2018;47:1098–1131.
11. Ma D-L, Zhang Z, Wang M, Lu L, Zhong H-J, Leung C-H. Recent developments in G-quadruplex probes. *Chem Biol.* 2015;22:812–828.
12. Vummidi BR, Alzeer J, Luedtke NW. Fluorescent probes for G-quadruplex structures. *ChemBioChem.* 2013;14:540–558.
13. Lu YJ, Guo XL, Xu MH, et al. Selective visualization of DNA G-quadruplex structures in live cells with 1-methylquinolinium-based molecular probes: the importance of indolyl moiety position towards specificity. *Dyes Pigm.* 2017;143:331–341.
14. Peng D, Tan J-H, Chen S-B, Ou T-M, Gu L-Q, Huang Z-S. Bisaryldiketene derivatives: a new class of selective ligands for c-myc G-quadruplex DNA. *Bioorg Med Chem.* 2010;18:8235–8242.
15. Liu Z-Q, Zhuo S-T, Tan J-H, et al. Facile syntheses of disubstituted bis(vinylquinolinium)benzene derivatives as G-quadruplex DNA binders. *Tetrahedron.* 2013;69:4922–4932.
16. Chung WJ, Heddi B, Hamon F, Teulade-Fichou M-P, Phan AT. Solution structure of a g-quadruplex bound to the bisquinolinium compound phen-DC3. *Angew Chem Int Ed.* 2014;53:999–1002.
17. De Cian A, DeLemos E, Mergny J-L, Teulade-Fichou M-P, Monchaud D. Highly efficient G-quadruplex recognition by bisquinolinium compounds. *J Am Chem Soc.* 2017;129:1856–1857.
18. Yang P, De Cian A, Teulade-Fichou M-P, Mergny J-L, Monchaud D. Engineering bisquinolinium/thiazole orange conjugates for fluorescent sensing of G-quadruplex DNA. *Angew Chem Int Ed.* 2009;28:2188–2191.
19. Dhamodharan V, Harikrishna S, Jagadeeswaran C, Halder K, Pradeepkumar PI. Selective G-quadruplex DNA stabilizing agents based on bisquinolinium and bispyridinium derivatives of 1,8-naphthyridine. *J Org Chem.* 2012;77:229–242.
20. Bolden S, Boateng CA, Zhu XY, et al. CoMFA studies and in vitro evaluation of some 3-substituted benzylthio quinolinium salts as anticryptococcal agents. *Bioorg Med Chem.* 2013;21:7194–7201.
21. Wang M-Q, Zhu W-X, Song Z-Z, Li S, Zhang Y-Z. A triphenylamine-based colorimetric and fluorescent probe with donor–bridge–acceptor structure for detection of G-quadruplex DNA. *Bioorg Med Chem Lett.* 2015;25:5672–5676.
22. Wang MQ, Ren GY, Zhao S, et al. Development of a carbazole-based fluorescence probe for G-quadruplex DNA: the importance of side-group effect on binding specificity. *Spectrochim Acta A.* 2018;199:441–447.
23. Wang MQ, Wu Y, Wang ZY, et al. G-quadruplex DNA fluorescence sensing by a bisamine-substituted styrylquinolinium dye. *Dyes Pigm.* 2017;145:1–6.
24. Patrick MJ, Ernst LA, Waggoner AS, Thai D, Taic D, Salamac G. Enhanced aqueous solubility of long wavelength voltage-sensitive dyes by covalent attachment of polyethylene glycol. *Org Biomol Chem.* 2007;5:3347–3353.
25. Bohländera PR, Wagenknecht HA. Synthesis and evaluation of cyanine–styryl dyes with enhanced photostability for fluorescent DNA staining. *Org Biomol Chem.* 2013;11:7458–7462.
26. Stootman FH, Fisher DM, Rodger A, Aldrich-Wright JR. Improved curve fitting procedures to determine equilibrium binding constants. *Analyst.* 2006;131:1145–1151.
27. Trott O, Olson AJ. AutoDock Vina: improving the speed and accuracy of docking with a new scoring function, efficient optimization, and multithreading. *J Comput Chem.* 2010;31:455–461.
28. Mishra A, Behera RK, Behera PK, Mishra BK, Behera GB. Cyanines during the 1990s: a review. *Chem Rev.* 1990;100(2000):1973–2011.
29. Song B, Zhang Q, Ma WH, Peng XJ, Fu XM, Wang BS. The synthesis and photostability of novel squarylium indocyanine dyes. *Dyes Pigm.* 2009;82:396–400.
30. Pordel M, Chegini H, Ramezani S, Daee M. New fluorescent heterocyclic systems from imidazo[1,2-a]pyridine: design, synthesis, spectral studies and quantum-chemical investigations. *J Mol Struct.* 2017;1129:105–112.
31. Monchaud D, Allain C, Teulade-Fichou MP. Development of a fluorescentintercalator displacement assay (G4-FID) for establishing quadruplex-DNAaffinity and selectivity of putative ligands. *Bioorg Med Chem Lett.* 2006;16:4842–4845.
32. Cheng XH, Liu XJ, Bing T, Cao ZH, Shangguan DH. General peroxidase activity of G-Quadruplex-hemin complexes and its application in ligand screening. *Biochemistry.* 2009;48:7817–7823.